

# Simulation and analysis of 60 GHz MMW for localisation based on machine learning

Mingwu Dou<sup>1</sup>, Wenwu Zhang<sup>2</sup>

<sup>1</sup>Fundamental Computer Department, Ocean University of China, Qingdao 266100, People's Republic of China

<sup>2</sup>Department of Computer Science and Technology, Ocean University of China, Qingdao 266100, People's Republic of China  
E-mail: 1994014@ouc.edu.cn

Published in *The Journal of Engineering*; Received on 19th June 2017; Accepted on 5th October 2017

**Abstract:** The 60 GHz pulse is more practical for the indoor localisation system due to its better time resolution. Usually, time-of-arrival (TOA) estimation with higher accuracy is critical to the indoor localisation. To acquire precise TOA estimations, a novel threshold crossing technique using neural network (NN) is discussed via analysing the characteristics of the received pulses based on the energy detection receiver. The relationship between the optimum thresholds and the signal-to-noise ratios (SNRs) are researched. Meanwhile, the influences caused by changing integration periods and channel models are examined. Results show that the proposed NN method can provide better accuracy and robustness to the lower SNR in the models designed by TG 3c.

## 1 Introduction

Wireless communications in 60 GHz band is a promising technique, which can achieve a transmission rate of Gbps for wireless networks due to its better anti-interference ability, the development of low-cost complementary metal-oxide-semiconductor devices etc. Federal Communications Commission (FCC) permits that the effective isotropic radiated power in the 60 GHz communication can be up to 40 dBm. Although the 60 GHz pulse attenuation is higher than other signals in low-frequency band, the power of the received pulses is still significant. Impulse-radio technique has been widely used in indoor positioning by using the 60 GHz signal due to its high time and multipath resolutions. The pulse provides better multipath resolution required for the accurate positioning [1]. As a result, the 60 GHz pulses are suitable for the indoor localisation applications in short range [2].

Usually, two major methods are used for the localisation including the time-based methods, e.g. the time-of-arrival (TOA) and time-difference-of-arrival, and the non-time-based methods, e.g. received-signal-strength, and angle-of-arrival (AOA). The positioning technique using time delay is more suitable for the 60 GHz pulse strategy due to its higher time resolution. TOA estimation with high accuracy is critical to acquire accurate indoor positioning, which is usually difficult to achieve due to the multipath components especially in non-line-of-sight (NLOS) scenes [3]. For the past few years, TOA methods have been widely discussed [4–10]. Two approaches are usually used to achieve TOA estimation including a matched filter (MF) with Nyquist sampling frequency and the energy detection (ED) with low sampling rate. Compared to the MF, an ED is a better scheme for TOA estimation, which only contains a square device, an integrator, a sampler and a decision mechanism as shown in Fig. 1. TOA can be estimated via comparing the integrator outputs with a better threshold value obtained based on the received pulses. Meanwhile, the priori channel estimation is not required for the ED.

How to determine a suitable threshold is the most difficult problem of the ED receiver according to the received pulses. In [5], the threshold was determined via analysing the kurtosis characteristics of the pulses. In [6], a method was discussed based on the ratio of the minimum to the maximum samples. However in low signal-to-noise ratio (SNR) conditions, all these algorithms cannot obtain precise TOA estimation, which limits the localisation accuracy due to the effective path cannot be identified.

The neural network (NN) has been extensively used for wireless communication and signal analysis [4]. To minimise the error

between different layers, the biases and weights can be automatically adjusted according to the training results. Owing to the complex scenes in indoor wireless communication, it is challenging to acquire the closed-form solutions, which can be used to acquire TOA estimations. In this paper, the back-propagation NN (BPNN) is used to resolve a regression problem with a joint metric  $G$  values being the inputs and the optimum thresholds being the outputs, which has the ability to supply a better mapping according to the training results. The relationships between SNR and the characteristics of the received pulses such as the kurtosis and the skewness are considered. A parameter is developed using the characteristics of the received 60 GHz pulses, which is critical to the threshold determination. For every SNR value, the related thresholds are discussed and the influences on TOA estimation caused by the changing integration periods and propagation models are validated. Simulations are made to validate the better performances and strong robustness of the new method in different scenes such as LOS and NLOS conditions.

This paper is constructed as Section 2 introduces the model for 60 GHz communication. Several threshold crossing (TC) algorithms are discussed in Section 3. Section 4 analyses the calculated characteristics of the 60 GHz pulses. In Section 5, the optimum normalised threshold was determined in different scenes. A novel TC algorithm for TOA estimation is developed using BPNN in Section 6. Results are given in Section 7 compared with several well known methods. Moreover, this paper is concluded in Section 8.

## 2 Mathematical model

Two major channel models were developed for 60 GHz wireless communication system such as 3c models and 11ad models. The 3c standard was used in this paper, which was developed for wireless personal area network specifically. In this paper, a pulse position modulation (PPM) and time hopping (TH) 60 GHz pulse is used to estimate TOA [2].

### 2.1 60 GHz pulse

The transmitted 60 GHz pulse is given by

$$S(t) = \sum_{-\infty}^{\infty} p(t - jT_s - C_jT_c - a_j\epsilon) \quad (1)$$

where  $T_s$  stands for the symbol time,  $C$  stands for the TH code,  $T_c$  stands for the chip time,  $\epsilon$  stands for the PPM delay, the delay is  $\epsilon$

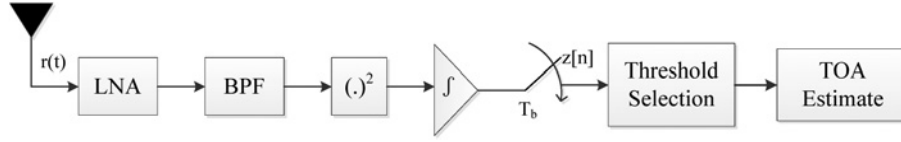


**Fig. 1** Block diagram of the conventional ED receiver

when  $a_j = 1$ . Usually the mentioned parameters must satisfy

$$C_j T_c + \varepsilon < T_s \quad (2)$$

$$\varepsilon < T_c \quad (3)$$

$$a_j \varepsilon < C_j T_c (C_j \neq 0) \quad (4)$$

Several different pulse waveforms have been designed in 60 GHz system. In this paper, the employed pulse is expressed as

$$p(t) = \frac{\sqrt{2}}{\beta} e^{(-2\pi^2/\beta^2)} \cos(2\pi f_c t) \quad (5)$$

where  $\beta$  stands for the pulse shape factor and  $f_c$  stands for the carrier frequency.

## 2.2 Signal attenuation

The path loss is key to analyse the link budget, which can be calculated based on the ratio of the power of the received pulses to the power of the transmit pulses. Different from the existing narrow-band systems, the path loss is dependent on both the frequency and the range in a wideband system. However, the path loss is usually considered as the functions of the range. As a result, the path loss, which is only dependent on the range, can be expressed as

$$PL_{(d)} = 10 \cdot n \log_{10} \left( \frac{d}{d_0} \right) + PL_0 + X_\sigma; \quad d \geq d_0 \quad (6)$$

where  $d_0$  and  $d$  stand for the reference range and the real propagation range, respectively.  $n$  stands for the pulse exponents of the path loss and  $X_\sigma$  stands for a Gaussian random variable with unit decibels.

The propagation delay of the 60 GHz pulse can be given by

$$\hat{\tau} = dt \times \left[ \frac{d}{c} \times \frac{1}{dt} \right] \quad (7)$$

where  $d$  stands for the propagation range between the target node and the reference node,  $(1/dt)$  stands for the sampling frequency, and  $c = 3 \times 10^8$  m/s stands for the speed of the light.

## 2.3 Multipath loss

The received pulses are given by

$$r(t) = \sum_{n=1}^N \alpha_n p(t - \tau_n) + n(t) \quad (8)$$

where  $N$  stands for the multipath number,  $\alpha_n$  stands for the amplitude of the  $n$ th propagation path, while  $\tau_n$  stands for the related time delay,  $p(t)$  stands for the transmitted 60 GHz signals, and  $n(t)$  stands for the Gaussian noise. Equation (8) is represented as in another form

$$r(t) = h(t)^* s(t) + n(t) \quad (9)$$

where  $h(t)$  stands for the model realisations given by

$$h(t, \varphi) = \sum_{k=1}^K \sum_{l=1}^{L_k} \mu_{kl} \delta(t - T_k - \tau_{kl}) \delta(\varphi - \varphi_k - \varphi_{kl}) \quad (10)$$

where  $\delta(\cdot)$  stands for a Dirac delta function,  $K$  stands for the cluster number,  $k$  stands for the  $k$ th clutter, and  $l$  stands for the  $l$ th ray,  $L_k$  stands for the number of the rays,  $kl$  stands for the  $l$ th ray of the  $k$ th cluster,  $\mu_{kl}$  stands for the amplitude,  $\omega_{kl}$  stands for the azimuth, and  $\tau_{kl}$  stands for the time delay,  $T_k$  stands for the mean propagation time, and  $\theta_k$  stands for the average AOA.

## 2.4 ED receiver

The 60 GHz pulses are squared after the amplifier, and then the outputs of the ED can be given by

$$z[n] = \sum_{i=1}^N \int_{(i-1)T_f + (c_j+n-1)T_b}^{(i-1)T_f + (c_j+n)T_b} r^2(t) dt \quad (11)$$

where  $n \in \{1, 2, \dots, N\}$  stands for the indexes of the acquired samples,  $N$  stands for the pulse number in each symbol,  $T_b$  stands for the integration period,  $(3T_f/2)$  stands for the integration duration, which is used to account for the inter-frame leakage due to the multipath signals,  $N = (3T_f/2T_b)$  stands for the number of the acquired samples. In this paper,  $N = 1$ . Moreover, the outputs are

$$z[n] = \int_{(c_j+n-1)T_b}^{(c_j+n)T_b} r^2(t) dt \quad (12)$$

If  $z[n]$  only contains Gaussian noise, it follows the central chi-square distribution, and it follows a non-central chi-square distribution when the effective pulses present. For the central chi-square function, the mean and variance can be given by

$$\mu_0 = F\sigma^2, \quad \sigma_0 = 2F\sigma^4 \quad (13)$$

Moreover, for the non-central chi-square function, it follows:

$$\mu_e = F\sigma^2 + E_n, \quad \sigma_e^2 = 2F\sigma^4 + 4\sigma^2 E_n \quad (14)$$

where  $E_n$  is for the pulse energy and  $F$  is for the degrees of freedom, which can be given by

$$F = 2 \times W \times T_b + 1 \quad (15)$$

where  $W$  stands for the effective bandwidth of the pulse.

## 3 ED-based TOA estimation

Many TOA estimation techniques using an ED receiver have been discussed to estimate the first arriving block using the received pulses. The maximum energy selection (MES) method was considered as the simplest TOA estimation method, which tries to detect

the maximum energy value. Moreover, TOA can be estimated as

$$\tau_{\text{MES}} = \arg \max_{1 \leq n \leq N} \{z[n]\} \times T_b - \frac{1}{2} \times T_b \quad (16)$$

As shown in Fig. 2, the propagation path did not exist in the maximum energy particularly in NLOS scenes. It can be seen that the energy  $z[n]$  containing the first arriving path is located before  $z[n]_{\text{max}}$ . As a result, the TC method was developed using an ED receiver, where the calculated energy samples are used to compare with a better threshold  $\alpha$ . TOA can be estimated as

$$\tau_{\text{TC}} = \arg \min_{1 \leq n \leq N} \{n | z[n] \geq \alpha\} \times T_b - \frac{1}{2} \times T_b \quad (17)$$

However, it is changing to acquire a suitable threshold  $\alpha$  directly. As a result, the normalised threshold  $\alpha_{\text{norm}}$  is defined, and  $\alpha$  can be calculated as

$$\alpha = \alpha_{\text{norm}} [z[n]_{\text{max}} - z[n]_{\text{min}}] + z[n]_{\text{min}} \quad (18)$$

Moreover, then  $\tau_{\text{TC}}$  can be acquired based on (14). The fitted threshold method is considered as one of the simpler TC methods, i.e.  $\alpha_{\text{norm}}$  is considered as a fixed value. At this moment, the problem is how to acquire a normalised threshold based on the received pulses.

Usually, the mean absolute error (MAE) calculated from the TOA estimation was used to analyse the performances of the TC method, which can be given by

$$\text{MAE} = \frac{1}{N} \sum_{n=1}^N (t_n - \hat{t}_n) \quad (19)$$

where  $t_n$  for the  $n$ th real time delay and  $\hat{t}_n$  for the  $n$ th TOA estimation.

## 4 Signal characteristics

The characteristics including the skewness and the kurtosis of the received pulses will be discussed in this section.

### 4.1 Kurtosis

For the calculated energy samples, the kurtosis can be given by

$$k = \frac{E[(z(n) - \mu)^4]}{E[(z(n) - \mu)^2]^2} = \frac{E[(z(n) - \mu)^4]}{\sigma^4} \quad (20)$$

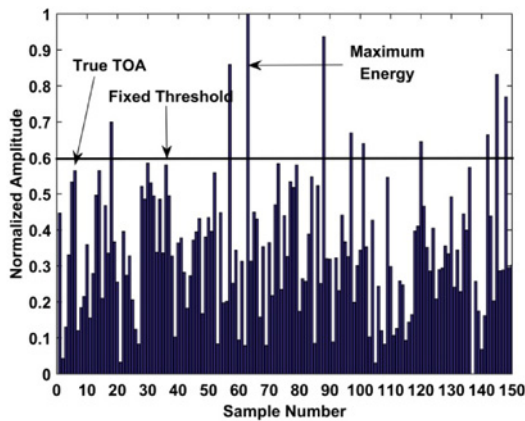


Fig. 2 TOA estimation using MES and the fixed threshold

where  $\mu$  for the mean of the received pulses and  $\sigma$  stands for the standard deviation.

In this paper, the excess kurtosis is used to analyse the signals, which is given by

$$\tilde{k} = k - 3 \quad (21)$$

Usually, as SNR increases,  $\tilde{k}$  increases.

### 4.2 Skewness

For the calculated energy samples, the skewness can be expressed as

$$s = \frac{1}{(N-1)\delta^3} \sum_{i=1}^N (z(n) - \mu)^3 \quad (22)$$

Usually, as SNR increases,  $s$  increases.

### 4.3 Characteristics analysis

In this section, the statistical characteristics of the received pulses are analysed via employing the indoor residential models including the CM1.1 (LOS) and CM2.1 (NLOS) models provided by the 3c standard. The SNR changed in the range 4–34 dB, and for every SNR value, 1000 realisations are obtained with the sampling frequency  $f_s = 10$  GHz. The other key parameters for the simulation system are  $T_f = 200$ ,  $T_c = 1$ , and  $T_b = 1$  ns. Each realisation follows the uniformly distributed within  $(0 - T_f)$ .

As shown in Fig. 3, the characteristics of the energy blocks are acquired in both NLOS and LOS models. Results indicate that the characteristics with respect to SNR are similar in both LOS and NLOS models. Here, ‘S/K’ denotes the ratios of the skewness to the kurtosis and ‘K/S’ denotes the ratios of the kurtosis to the skewness. As shown in Fig. 3, it can be seen that ‘K/S’, kurtosis, and skewness increases with SNR increases, ‘K/S’ increases more quickly than the other parameters. However, the ‘S/K’ decreases with SNR increases. Compared to other parameters, the ‘K/S’ increases more quickly, which are more suited to reflect the changing SNR. Moreover, it can also be seen that the ‘K/S’ increases slightly, whereas the ‘S/K’ decreases more quickly when  $\text{SNR} < 12$  dB. However, the ‘K/S’ increases more quickly while the ‘S/K’ decreases slightly when  $\text{SNR} > 12$  dB. As a result, no single parameter is suited to reflect the changing SNR. Given the fact, a new parameter using the ‘K/S’ and the ‘S/K’ is proposed for TOA estimation, which can be given by

$$G = K/S - S/K \quad (23)$$

## 5 Optimum threshold

To train the NN, the relationships between the new parameter  $G$  and the optimum threshold  $\alpha_{\text{opt}}$  have to be examined. As shown in Fig. 4, the curves are similar in both NLOS and LOS for the given  $T_b$ , in this paper, only  $T_b = 1$  and 4 ns are considered. To determine the relationships, the steps can be summarised as follows:

- (i) About 1000 channel realisations are acquired in LOS and NLOS models with  $T_b = 1$  and 4 ns, and SNR changes within 4–34 dB.
- (ii) The average MAEs are calculated related to different  $\alpha_{\text{norm}}$  acquired from different  $G$  values, channel model, and  $T_b$ . In the simulation, different MAE values can be acquired for each given normalised threshold due to the generated pulses randomly. As a result, the average MAE is calculated for each given threshold. Meanwhile,  $G$  was rounded to the half integer and integer values for each given SNR.

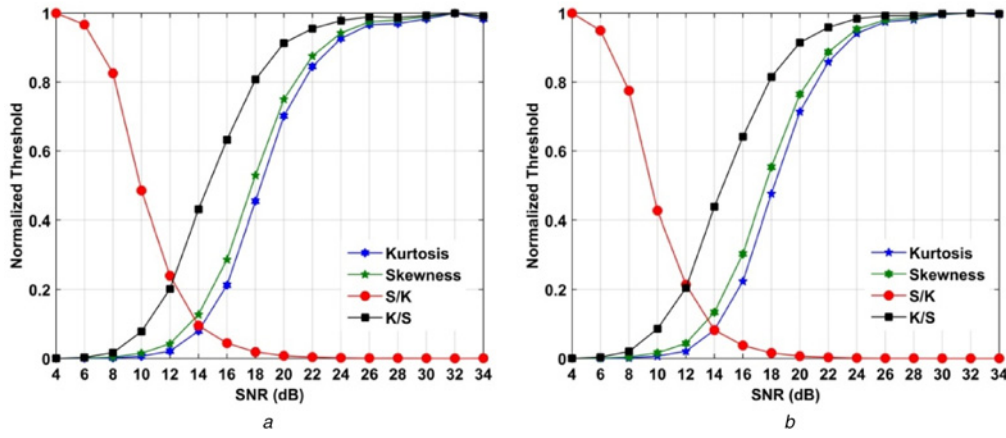


Fig. 3 Relationship between the SNR and the characteristics with  $T_b = 1$  ns  
a CM1.1  
b CM2.1

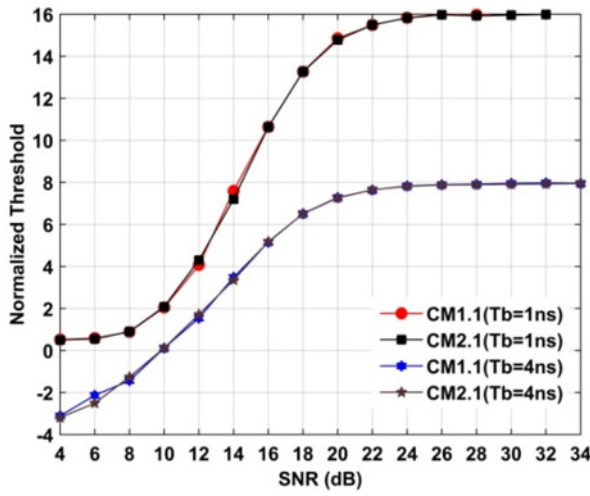


Fig. 4 Mean  $G$  values related to SNR with different models and  $T_b$

- (iii) The normalised thresholds related to the MAE are considered as the better threshold  $\alpha_{\text{better}}$  for each rounded  $G$  with different models and  $T_b$ .
- (iv) The average  $\alpha_{\text{better}}$  in NLOS and LOS for each given  $G$  are considered as the optimum  $\alpha_{\text{norm}}$ , i.e.  $\alpha_{\text{opt}}$ .

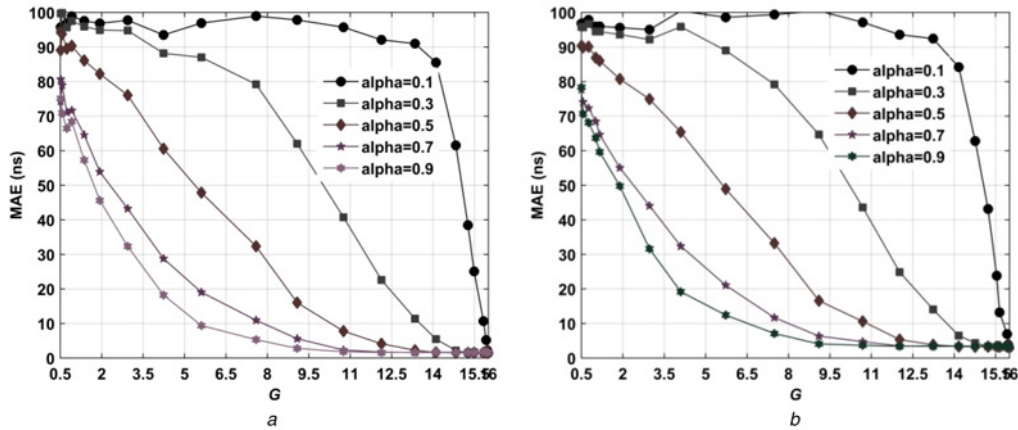


Fig. 5 Relationship between  $G$  and MAE with  $T_b = 1$  ns  
a CM1.1  
b CM2.1

To validate the relationships between the new parameter  $G$  and the related SNR, 1000 realisations are acquired with SNR being 4–34 dB in both LOS and NLOS models. The relationship between the  $G$  and SNR was presented in Fig. 4. It can be seen that the new parameter  $G$  is a monotonic function of the SNR. Compared to the single parameter,  $G$  is more suited to reflect the changing SNR.

To determine  $\alpha_{\text{better}}$  for each given  $G$ , the relationships between the normalised threshold  $\alpha_{\text{norm}}$  and the calculated MAE are examined. Via simulations, the acquired relationships in LOS and NLOS models are shown in Fig. 5. It can be seen that the average MAE is a monotone decreasing function of the  $G$  values. In this paper, the  $\alpha_{\text{norm}}$  related to the minimum MAE is considered as  $\alpha_{\text{better}}$  for every determined SNR. Results show that the relationships may be affected by the changing models, but it is dependent on  $T_b$ . As a result,  $\alpha_{\text{opt}}$  is given by

$$\alpha_{\text{opt}}^{(T_b=\text{ins})}(G) = \frac{\alpha_{\text{better}}^{(\text{CM1.1}, T_b=\text{ins})}(G) + \alpha_{\text{better}}^{(\text{CM2.1}, T_b=\text{ins})}(G)}{2} \quad (24)$$

Fig. 6 shows the optimum thresholds acquired from the best threshold values with  $T_b = 1$  and 4 ns.

## 6 Threshold selection using NN

In this section, the NN-based TC method is analysed. The NN is shown in Fig. 7, which only contains three parts. The weights

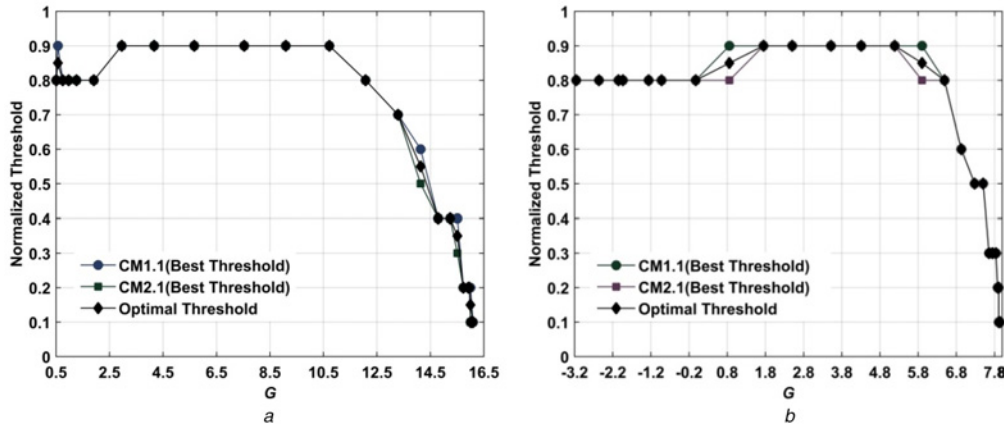


**Fig. 6** Normalised thresholds with respect to  $G$   
a  $T_b = 1$  ns  
b  $T_b = 4$  ns

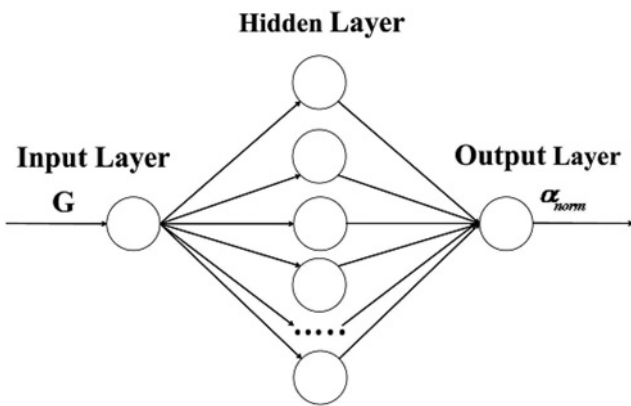


**Fig. 7** Structure of the BPNN employed in this paper

between two layers can be adjusted based on the calculated errors using the inputs and outputs. However, it is usually challenging to determine the neuron number of the hidden layer [11]. Many methods for initialising and training NN have been discussed in recent years. The initialised technique discussed in [10] was used to initialise the weights and biases of the NN in this paper. The neuron number in the hidden layer is critical to the success of training NN. Enough information cannot be acquired to solve problems when only a few neurons exist in the hidden layer. However, the time spent on training NN will be long enough when too many neurons exist in the hidden layer, which can also cause the over-fitting problem. The neuron number can be determined based on the mean squared error (MSE) acquired from the training results when NN is trained 200 times repeatedly [4]. Using the method in [4], the following conclusions can be acquired as below.

For  $T_b = 1$  ns, when 28 neurons exist in the hidden layer, more than 95% MSE values are  $< 1 \times 10^{-10}$  and then changes slightly even continue to increase the neuron number. As a result, 28 neurons exist in the hidden layer for the proposed NN.

For  $T_b = 4$  ns, when 24 neurons exist in the hidden layer, more than 95% MSE values are  $< 1 \times 10^{-10}$  and then changes slightly even continue to increase the neuron number. As a result, 28 neurons exist in the hidden layer for the proposed NN.

To decrease complexity of the computation in determining the neuron number, and improve the effectiveness, the neuron number is determined according to the acquired training results that the least MSE up to the level  $1 \times 10^{-10}$  for the first time. As a result, the neuron number can be estimated as below.

For  $T_b = 1$  ns, the least MSE is  $1.97 \times 10^{-32}$  when 14 neuron numbers exist in the hidden layer. As a result, 14 neurons exist in the hidden layer for the proposed NN.

For  $T_b = 4$  ns, the least MSE is  $2.87 \times 10^{-33}$  when 12 neuron numbers exist in the hidden layer. As a result, 12 neurons exist in the hidden layer for the proposed NN.

$\alpha_{\text{norm}}$  usually changes within 0 to 1. As a result, the function  $1/(1 + e^{(-x)})$  is selected as the transfer function between different layers. To train NN, the Levenberg–Marquardt method is used to update the weights and bias values. There are only 28 ( $\alpha_{\text{norm}} - G$ ) including one input parameter and one output parameter in the proposed BPNN, and the requirement is modest.

### 6.1 NN training

To train NN, 1000 realisations for each given SNR within 4–34 dB are acquired for  $T_b = 1$  and 4 ns. Fig. 8 shows the optimum thresholds and the estimated thresholds based on the training results.

The integer  $G$  values within 1–16 for  $T_b = 1$  ns, and  $-3$  to 8 for  $T_b = 4$  ns, were used to train the proposed NN. The training results are given in Fig. 8. It can be seen that the acquired results are in almost total agreement with the optimum thresholds. For each given  $T_b$ , 1000 iterations are carried out in training the BPNN, and the one related to the minimum MSE is considered as the optimum NN. On the other hand, the half integer  $G$  values within 0.5–15.5 for  $T_b = 1$  ns and  $-2.5$  to 7.5 for 4 ns are used to validate the acquired optimum BPNN.

### 6.2 Validation results

To evaluate the performance of the trained BPNN, the  $G$  values within 1.5–15.5 with  $T_b = 1$  ns and  $-3.5$  to 7.5 with 4 ns are input to BPNN to get threshold estimations. As shown in Fig. 9, the two MSEs acquired from the two validations with  $T_b = 1$  and 4 ns are  $3.41 \times 10^{-16}$  and  $9.86 \times 10^{-33}$ . It can be seen that the outputs from the trained NN fit well with the optimum thresholds. As a result, there is reason to believe that the trained NN can provide any values for each given  $G$ . BPNN can also be used to eliminate the complexed and time-consuming optimisation process. Our BPNN can fit any model and scene and only the parameters between different layers are adjusted, which is particularly fit for the stationary model.

## 7 Results

To show the capability of improving TOA estimation accuracy, the MAEs are calculated with different ED-based TC methods in CM1.1 and CM2.1 channel models. A 60 GHz pulse with



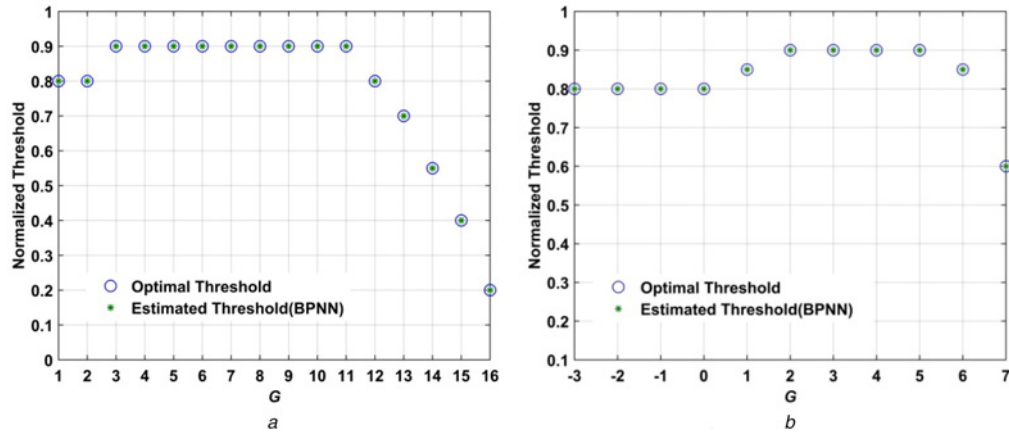


**Fig. 8** Training results for the NN

a  $T_b = 1$  ns

b  $T_b = 4$  ns

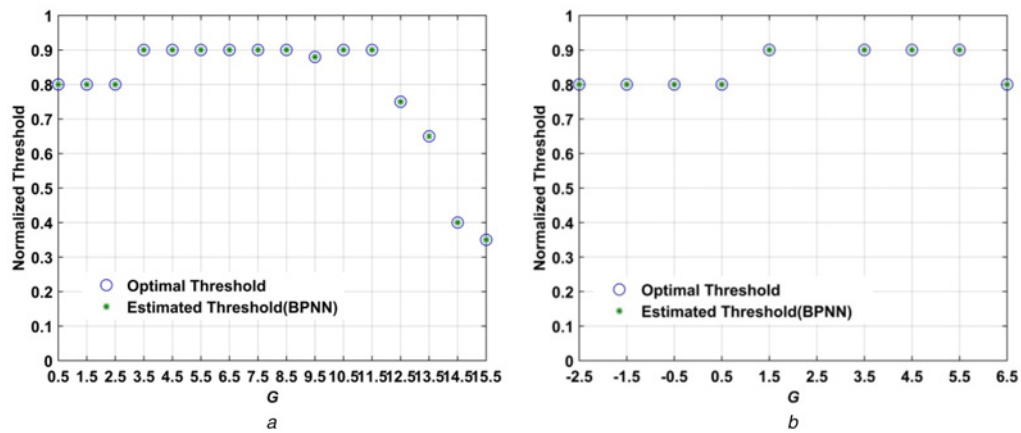


**Fig. 9** External validation of the trained NN

a  $T_b = 1$  ns

b  $T_b = 4$  ns

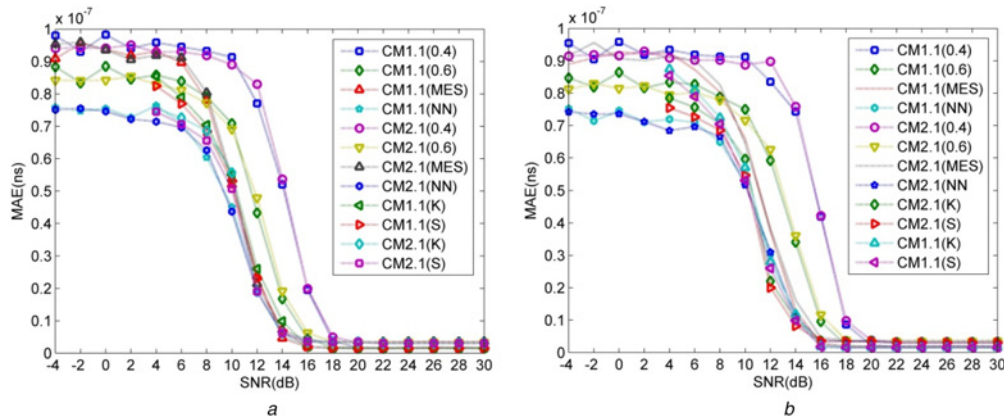


**Fig. 10** MAEs with different algorithms  $T_b = 1$  ns and 4 ns

a CM1.1

b CM2.1

PPM-TH modulated is employed, and the key parameters for simulations are set same as mentioned above.

The calculated MAEs in LOS models for each SNR within 4–34 dB are given in Fig. 10a. Moreover, the MAEs in NLOS are shown in Fig. 10b. It can be seen that the NN-based method outperforms the other algorithms. The TOA estimations in LOS are

more accurate than that acquired in NLOS models for the same  $T_b$ . Meanwhile, it can be seen that the TOA estimations are much more accurate for  $T_b = 1$  ns than 4 ns, which is irrelevant to the propagation model. The calculated MAEs via employing six ED-based TOA estimation methods in NLOS and LOS models are given in Fig. 10. It can be seen that the MAEs using the

BPNN method are much better than any other methods especially in low SNR. On the basis of the performances of the developed ED-based method, it is much more robust and adaptive than any other method. However, the differences are quite small among all these methods when  $\text{SNR} > 20$  dB. The proposed NN method performs more stably and provides more accurate TOA estimations especially for the low-SNR values than other methods.

In this section, 'K' denotes the TC method by analysing the kurtosis of the received signals, 'S' denotes the TC method by analysing the skewness of the received signals, 'MES' denotes the mentioned MES method, and the thresholds method for the fixed threshold (FT) method are set to be 0.4 and 0.6, respectively.

## 8 Conclusion

A new NN-based TC method for TOA estimation using an ED receiver is examined for 60 GHz positioning system. The characteristics of the received pulses are discussed and a new parameter is analysed using the skewness and the kurtosis for TOA estimation. The optimum thresholds were determined via simulation in NLOS and LOS models, and the influences caused by the changing integration periods and models are validated. Results show the performances of the NN-based method outperform several well known methods.

## 9 Acknowledgments

This work was funded by the National High Technology Research and Development Program of China (2012AA061403), the National Science & Technology Pillar Program during the 12th Five-year Plan Period (2014BAK12B00), the National Natural Science Foundation of China (61501424), and the Nature Science Foundation of China (41527901), the Major Program of China's Second Generation Satellite Navigation System (GF\*\*\*\*\*03), and the Fundamental Research Funds for the Central Universities (201713018).

## 10 References

- [1] Win M.Z., Scholtz R.A.: 'Energy capture vs. correlator resources in ultra-wide bandwidth indoor wireless communications channels'. Proc. IEEE MILCOM, Monterey, CA, November 1997, pp. 1277–1281
- [2] Liang X., Zhang H., Gulliver T.A.: 'Energy detector based time of arrival estimation using a neural network with millimeter wave signals', *KSII Trans. Internet Inf.*, 2016, **10**, (7), pp. 3050–3065, doi: 10.3837/tiis.2016.07.010
- [3] Hazra R., Tyagi A.: 'A survey on various coherent and non-coherent IR-UWB receivers', *Wirel. Pers. Commun.*, 2014, **79**, (3), pp. 2339–2369, doi: 10.1007/s11277-014-1988-4
- [4] Liang X., Zhang H., Lu T., *ET AL.*: 'Energy detector based TOA estimation for MMW systems using machine learning', *Telecommun. Syst.*, 2017, **64**, (2), pp. 417–427, doi: 10.1007/s11235-016-0182-2
- [5] Guvenc I., Sahinoglu Z.: 'Threshold selection for UWB TOA estimation based on kurtosis analysis', *IEEE Commun. Lett.*, 2005, **9**, (12), pp. 1025–1027, doi: 10.1109/LCOMM.2005.1576576
- [6] Guvenc I., Sahinoglu Z.: 'Multiscale energy products for TOA estimation in IR-UWB systems'. Proc. IEEE Global Telecommunications Conf., St. Louis, MO, January 2005, pp. 209–213
- [7] Guvenc I., Sahinoglu Z.: 'Threshold-based TOA estimation for impulse radio UWB systems'. Proc. IEEE Int. Conf. Ubiquitous Wireless Broadband, Zurich, Switzerland, October 2005, pp. 420–425
- [8] Khan M.G., Sallberg B., Nordberg J., *ET AL.*: 'Robust weighted non-coherent receiver for impulse radio UWB PPM signals', *IEEE Commun. Lett.*, 2011, **15**, (6), pp. 614–616, doi: 10.1109/LCOMM.2011.040711.102583
- [9] Feng W., Zhi T., Sadler B.M.: 'Weighted energy detection for noncoherent ultra-wideband receiver design', *IEEE Trans. Wirel. Commun.*, 2011, **10**, (2), pp. 710–720
- [10] Liang X., Zhang H., Lu T., *ET AL.*: 'Extreme learning machine for 60 GHz millimeter wave positioning', *IET Commun.*, 2017, **11**, (4), pp. 483–489, doi:10.1049/iet-com.2016.0080
- [11] Rowley H.A., Baluja S., Kanade T.: 'Neural network-based face detection', *IEEE Trans. Pattern Anal.*, 1998, **20**, (1), pp. 203–208, doi: 10.1109/34.655647